Electrical spin injection in metallic mesoscopic spin valves

Jedema, Friso

Chapter 2

Theory of spin polarized electron transport

2.1 Introduction

In general there are different theoretical transport formalisms which can be used to describe transport, ranging from the most simple, but transparent, free electron model, to complex 'ab initio' transport calculations where the physics can be difficult to interpret due the rigorous applied mathematical frameworks [1]. Ab initio calculations are characterized by the fact that no empirical parameters are used in the calculation and only the position of the atoms enter. The appropriate formalism to describe transport is determined by the transport regime applicable to a given experimental system or device. This usually depends on the characteristic physical length scale involved versus the size of the experimental system or device. The size of the metallic device structures as studied in this thesis are much larger than the elastic mean free path. Therefore the transport regime applicable to our devices is the diffusive regime which is described by the Boltzmann transport formalism.

The second important length scale for spin dependent diffusive transport is the spin relaxation length, which expresses how far an electron can travel in a diffusive conductor before its initially known spin direction is randomized. As the spin relaxation length in metals is usually much larger than the elastic mean free path, the transport can be described in terms of two independent diffusive spin channels. This 'two current transport model' [2–4] has been applied to describe transport in ferromagnetic metals [5–8], to describe transport across a F/N interface [9] and to explain the current perpendicular to plane (CPP) GMR effect, also known as the Valet-Fert (VF) model [10]. All mentioned approaches treat the nonmagnetic and ferromagnetic metals as free electron materials. Based on the the assumption that the elastic scattering time and the inter band scattering times are shorter

than the spin flip times (which is usually the case) the two current model is adequate to describe and explain the observed magnetoresistance effect in CPP-GMR multilayers. However, it is unable to quantify the bulk and interface spin asymmetry parameters and spin relaxation lengths as introduced in the VF model.

Understanding the physical origin of these parameters is currently an active field of research. Only recently for example Fabian and Das Sarma [11] have performed an ab initio band structure calculation to evaluate the spin relaxation time in elemental aluminum (Al), from which the spin relaxation length in Al can be deduced. The interfacial spin asymmetry parameters have been evaluated in diffusive Co/Cu and Fe/Cr multilayers in Refs. [1, 12–14], whereas bulk spin asymmetry parameters have been evaluated for diffusive fcc Co and bcc Fe bulk ferromagnetic metals in Ref.[15], as well as for diffusive Co/Cu and Fe/Cr multilayers .

2.2 Stoner ferromagnetism

In general magnetism originates from the spin of the electron, having a much larger magnetic moment than the nucleus of an atom. A net electron spin in an atom results from flexibility of ordering in the electronic arrangement of the electrons around the nucleus and the requirement for the electron wave function to obey the Pauli exclusion principle, that is: the complete wave function of a two or more electron system has to be antisymmetric with respect to the interchange of any two electrons. Therefore the symmetry (symmetric or antisymmetric) of the spin part of the wave function influences the symmetry of the spatial wave function and hence influences the total Coulomb energy of the electron system. The difference in energy between a two electron system with a symmetric (triplet) or antisymmetric (singlet) spin part of the wave function is referred to as the exchange energy E_{ex}. For example, ferromagnetism exists in iron (Fe), nickel (Ni) and cobalt (Co) atoms due the dependence of the Coulomb energy (the exchange energy) on the particular arrangement of the electrons and their spin in the 3d shell [16, 17]. It is intriguing to notice that these elements, having a nuclear charge of $Z = 26$, $Z = 27$ and $Z = 28$ respectively, have a magnetic moment, whereas the next element in the periodic table copper (Cu) with $Z = 29$ (and thus only 1 electron more) does not show any ferromagnetism. The reason is that Cu has a complete filled 3d shell, leaving no room for any flexibility in the electronic arrangement.

For the elementary ferromagnetic transition (3d) metals Fe, Ni and Co, the 'magnetically active' electrons have band-like properties, i.e. they are not bound to any particular nucleus. The Stoner criterium determines if a

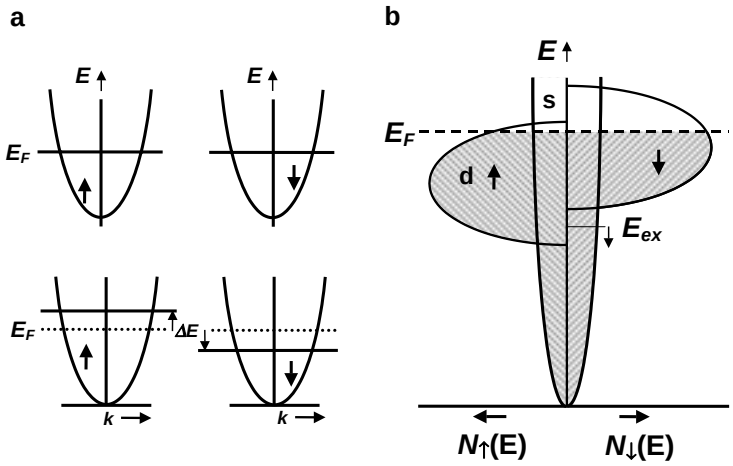

Figure 2.1: *(a) Schematic illustration to derive the Stoner criterium of ferromagnetism, see text. (b) Band structure of a ferromagnetic metal in the simple Stoner picture. The d spin sub-bands are shifted in energy due to the exchange interaction, leading to a finite magnetization and a difference in the densities of states ($N_\uparrow$, $N_\downarrow$) and Fermi velocities at the Fermi-energy (E_F).*

3d transition metal is stable against the formation of a ferromagnetic state, i.e. a Stoner ferromagnet or not. This criterium is schematically illustrated in Fig. 2.1a. Roughly, the Stoner model assumes energy bands, where the 3d-spin sub-bands are shifted with respect to each other due to the presence of the exchange interaction. For ferromagnetic ordering to occur the gain in exchange energy has to be larger than the increase in the kinetic energy [18]. Due to the exchange splitting of the d-bands, ferromagnetic metals exhibit a finite magnetization in thermodynamic equilibrium.

2.2.1 Electrical properties

A second effect of the exchange splitting is that the density of states (DOS) at the Fermi-energy (E_F) and the Fermi velocities become different for the two spin sub-bands. Due to the spin dependent DOS, Fermi velocities and scattering potentials, a ferromagnetic metal is characterized by different bulk conductivities for the spin-up and spin-down electrons:

$$\sigma_{\uparrow,\downarrow} = e^2 N_{\uparrow,\downarrow} D_{\uparrow,\downarrow} \text{ with } D_{\uparrow,\downarrow} = 1/3 v_{F\uparrow,\downarrow} l_{e\uparrow,\downarrow} \; . \tag{2.1}$$

Here $\sigma_{\uparrow,\downarrow}$ denotes the spin-up and spin-down conductivity, e is the absolute value of the electronic charge, $N_{\uparrow,\downarrow}$ is the spin dependent DOS at the Fermi energy, $D_{\uparrow,\downarrow}$ the spin dependent diffusion constant, $v_{F\uparrow,\downarrow}$ the average spin dependent Fermi velocity and $l_{e\uparrow,\downarrow}$ the average spin dependent electron mean free path. By definition, throughout this thesis, the spin-up ($\uparrow$)

electrons are related to the majority electrons which are determining the magnetization and the spin-down ($\downarrow$) electrons are related to the minority electrons. The bulk current polarization of a ferromagnetic metal is then defined as:

$$\alpha_F = \frac{\sigma_\uparrow - \sigma_\downarrow}{\sigma_\uparrow + \sigma_\downarrow} \,. \tag{2.2}$$

To quantify the magnitude of the current polarization is not a simple task, as it lies outside the scope of the free electron model. Even the sign of the bulk current polarization in ferromagnetic metals is not trivial as will be discussed in the next paragraph. However for the conventional ferromagnets (Fe, Co and Ni) the magnitude of α_F is expected to be in the range $0.1 < |\alpha_F| < 0.7$. Note that α_F is defined similarly as the parameter β in the VF model.

2.2.2 Spin polarization

This section is included to stress the difference of the current polarization in different experiments and transport regimes. Although for transport experiments the definition of polarization is always related to the current, the relevant physical quantities determining these (spin) currents can be very different [19].

Polarization of the conductivity of bulk ferromagnetic metals

Fert and Campbell used the idea of a two-current model [2–4] to describe transport properties of Ni, Fe and Co based alloys [5, 6]. The temperature dependence of binary Ni and Fe alloys and a deviation from the Matthiessen's rule in the residual resistivity of ternary alloys at low temperatures allowed them to extract the spin dependent resistivities of a given impurity (among them Ni, Fe and Co) in a Ni, Fe or Co host metal [7, 8]. They obtained very high spin asymmetry ratios $\rho_{0\downarrow}/\rho_{0\uparrow}$ for Fe ($\rho_{0\downarrow}/\rho_{0\uparrow} = 20$) and Co ($\rho_{0\downarrow}/\rho_{0\uparrow} = 30$) impurity resistivities in a Ni host metal [7]. Here $\rho_{0\uparrow}, \rho_{0\downarrow}$ are the spin-up and spin-down resistivities induced by the impurity in the host metal. However low spin asymmetry ratios were obtained for Ni ($\rho_{0\downarrow}/\rho_{0\uparrow} = 3$) and Co ($\rho_{0\downarrow}/\rho_{0\uparrow} = 1$) impurity resistivities in a Fe host metal [7]. This result is interesting as it shows that the spin dependent scattering in Ni, Fe and Co would produce a positive polarization α_F, using:

$$\alpha_F = \frac{\rho_{0\downarrow}/\rho_{0\uparrow} - 1}{\rho_{0\downarrow}/\rho_{0\uparrow} + 1} \,. \tag{2.3}$$

On the other hand it can be shown by a simple exercise that α_F is predicted to be negative when (spin dependent) scattering is disregarded. From band structure calculations in Ref. [20] the total spin dependent DOS and

average Fermi velocities can be obtained for Ni, being 2.51 states/Rydberg/atom and $0.76 \cdot 10^6 m/s$ for the majority (up) spin and 21.28 states/Rydberg/atom and $0.25 \cdot 10^6 m/s$ for the minority (down) spin. According to Eq. 2.1 these values and assuming $l_{e\uparrow} = l_{e\downarrow}$ would result in a negative α_F, the opposite as obtained from the extrapolation of the results in Ref. [7] via Eq. 2.3. A similar situation exists for fcc Co, where a negative polarization of the ballistic conductance is predicted by taking only the electronic band structure into account [13]. Ab initio band structure calculations which take into account spin-independent scattering predict a positive polarization α_F for fcc Co of about 60 % [15]. However, in Ref. [15] a negative polarization α_F of 30 % is obtained for bcc Fe. The close intertwining of electronic structure, spin independent and spin dependent scattering therefore prohibits a transparent picture, which can predict the sign of the polarization α_F, let alone its magnitude.

In Ref. [21] the current polarization of metallic Co is taken to be positive as a reference to other metals, as several theory papers predict it to be positive [15, 22, 23]. The measured magnitude of the current polarization of Co in CPP-GMR experiments is reported to be in the range $35 - 50$ % [21, 24–26]. For Py values are reported to be in the range of $65 - 80$% [27–29], having the same (positive) sign as Co [21]. The situation gets even more interesting for ferromagnetic metals doped with impurities. For instance, the sign of the (positive) polarization of bulk Ni can be made negative by adding only 2.5 at. % Cr [21], favoring a qualitative agreement with the spin asymmetry ratio $\rho_{0\downarrow}/\rho_{0\uparrow} < 1$ for Cr impurities in a Ni host [7, 21].

All spin valve experiments described in this thesis use the same ferromagnetic metal for spin injection as well as detection. Therefore no information about the sign of α_F can be obtained as α_F enters squared, via injector and detector, in the magnitude of the experimentally observed spin accumulation.

Interface polarization of transparent contacts

The interface polarization for transparent contacts between diffusive metals, as expressed by γ in the VF theory for a CPP-GMR multilayer geometry is defined as:

$$\gamma = \frac{R_\downarrow^{int} - R_\uparrow^{int}}{R_\downarrow^{int} + R_\uparrow^{int}} \,, \tag{2.4}$$

where $R_\uparrow^{int}$ and $R_\downarrow^{int}$ are the interface resistances of the spin-up and spin-down channels. The origin of the interface resistance between two different diffusive metals in a CPP-GMR multilayer geometry can be two fold. One ingredient is the electronic structure of the metals, which is labelled with

the term 'intrinsic potential' in Ref. [21]. The other contribution stems from disorder at the interface, such as intermixing, impurities and interface roughness and has been labelled with the term 'extrinsic potentials' in Ref. [21].

On the theoretical side progress has been made to resolve the different contributions to the total interface resistance. It was shown for Co/Cu multilayers that diffusive electron propagation through the bulk Co and Cu multilayers in combination with specular reflection at the interfaces could account for the experimentally observed values of $\gamma_{Co/Cu} \approx 70$ % [12, 21, 26, 30–32]. Including disorder at the Co/Cu interface did not change this result much [14]. Note however that the positive sign of the polarization is again different from the ballistic Sharvin conductance polarization for bulk fcc Co, which yields a negative value reflecting the higher minority DOS [13]. The sign change originates from the fact that the majority spin Co and Cu band structures are well matched, whereas this is not the case for the minority spin [13]. For Fe/Cr multilayers the interface resistance of the majority spin is larger and hence a negative spin polarization γ is obtained, ranging from 30 % to 70 % for disordered and clean interfaces respectively [14].

Experimentally it has been very difficult to discriminate between the 'intrinsic' and 'extrinsic' interface resistance contributions [21]. To complicate things even further, a recent attempt has revealed that not the impurities at the interface of Co/Cu multilayers seem to matter for the CPP-GMR effect, but rather 3d ferromagnetic dopants in the bulk Cu layers and Cu impurities in the bulk Co layers [33].

Interface polarization of tunnel barrier contacts

For the polarization of ferromagnetic tunnel barrier contacts the situation is even more complex and spectacular. The tunnelling spin polarization P for a F/I/N tunnel barrier junction is defined as:

$$P = \frac{G_{\uparrow}^{TB} - G_{\downarrow}^{TB}}{G_{\uparrow}^{TB} + G_{\downarrow}^{TB}} \,, \tag{2.5}$$

where $G_{\uparrow}^{TB}$ and $G_{\downarrow}^{TB}$ are the tunnel barrier conductivities of the spin-up and spin-down channels. This definition corresponds to the definition of the electrode spin polarization used in the Julliere model describing the tunnel magnetoresistance (TMR) effect of F/I/F junctions [34, 35] and also corresponds to the definition of the polarization of F/I/S junction in the work of Tedrow and Meservey [36]. Positive spin polarizations for F/Al_2O_3/S tunnel barrier junctions were obtained in Ref. [36] for Fe, Co and Ni ferromagnetic electrodes yielding values of 40 %, 35 % and 23 % respectively.

The sign of the polarization can be determined in F/I/S junctions, because the magnetic field direction splitting the DOS of the Al superconductor is known. Note that this positive sign is again counter intuitive in relation with the higher DOS for the minority $\downarrow$ electrons.

Later work on magnetic F/I/F tunnel junctions (MTJ) showed that the polarization P can be 'tuned' from positive to negative. In Co/Al_2O_3/Co junctions the sign of the electrode polarization P could be reversed from positive to negative by inserting a fraction of a Ru monolayer in between the Co electrode and Al_2O_3 tunnel barrier. This effect was attributed to a strong modification of the local DOS at the Co/Ru interface [37]. Furthermore, the positive sign of the spin polarization P for a $Co/Al_2O_3/Al$ tunnel barrier changes into a negative polarization when the aluminum oxide is replaced by a strontium titanate or cerium lanthanite tunnel barrier [38]. This shows that the polarization of tunnel junctions not only depends on the thickness and effective height of the tunnel barrier [39], but also on the (local) DOS and the tunnel barrier material. For a detailed review and discussion on the nature of the spin polarization in MTJ's the reader is referred to Refs. [36, 40–42].

2.2.3 Anisotropic magnetoresistance

The resistivity of single ferromagnetic strips can be a few percent smaller or larger when the magnetization (**M**) is perpendicular to the current direction as compared to a parallel alignment. This effect is known as the anisotropic magnetoresistance (AMR) effect [43–45]. Changes in the resistance of a few percent are easily measurable, making it a sensitive way to monitor the magnetization direction and magnetization reversal processes of a submicron ferromagnetic strip.

AMR is a band structure effect and in Refs. [44, 46] it is argued that the microscopic origin relies on the anisotropic spin-orbit mixing of the spin-up and spin-down d bands accompanied by an anisotropic intra-band *sd* scattering probability, being largest for **M** parallel the **k** vector of the minority spin electrons. When both effects are taken into account the resistivity ρ of the ferromagnetic metal is usually found to be larger when **M** is parallel ($\rho_{||}$) to the direction of the current than in the situation where **M** is perpendicular to the direction of the current ($\rho_{\perp}$). The resistance difference $\rho_{||} - \rho_{\perp}$ is derived to be proportional to the square cosine of the angle Ψ between the current and **M** [44, 45]:

$$\rho_{||} = \rho_{\perp} + \Delta\rho \cdot cos^2(\Psi) \; . \tag{2.6}$$

The typical magnitude of $\Delta\rho$ for $Ni_{80}Fe_{20}$ (Py), Co and Ni metals is in the order of a few percent of $\rho_{\perp}$ and has a positive sign.

2.3 Spin injection and accumulation: the basic idea

Here the concept of spin injection and accumulation is introduced in a way similar to the pedagogical model introduced by Johnson & Silsbee [47] to describe the induced magnetization in a nonmagnetic metal. However one has to keep in mind that this description of spin injection and accumulation is only valid in the situation where a nonmagnetic metal is weakly coupled, i.e. via tunnel barriers, to its electrical environment. This is shown in detail in §2.6.

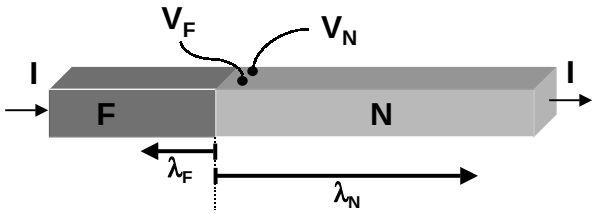

Figure 2.2: *Schematic representation of the experimental layout for electrical spin injection. A current* I *is flowing through a F/N interface. The arrows indicated with* λ_F *and* λ_N *on either side of the F/N interface represent the distance where the spin accumulation exists in the F and N metal. The spin accumulation can be probed by attaching a F and N voltage probe to N within a distance* λ_N *from the F/N interface.*

The first step is to the inject spins in a nonmagnetic metal by a ferromagnetic metal. This is realized by connecting a ferromagnetic strip (F) to a nonmagnetic strip (N), as is shown in Fig. 2.2. The current I is flowing perpendicular to the F/N interface and therefore the experimental geometry of Fig. 2.2 is related to the current perpendicular to the plane (CPP) GMR experiments where the current is flowing perpendicular to the planes of the F and N multilayers [1, 24, 48]. As the conductivities for the spin-up and spin-down electrons in a ferromagnetic metal are unequal, the usual charge current $(I_\uparrow + I_\downarrow)$ in F is accompanied by a spin current $(I_\uparrow - I_\downarrow)$ transporting magnetization in (or against) the direction of charge current. This makes a ferromagnetic metal an ideal candidate as an electrical source of spin currents for temperatures below the Curie temperatures.

When the electrons carrying the spin current $(I_\uparrow - I_\downarrow)$ have crossed the F/N interface from F to N, the conductivities for the spin-up and spin-down electrons are equal. This will cause the electron spins to pile up or accumulate over a distance λ_F and λ_N at either side of the F/N interface: the induced magnetization, see Fig. 2.3c. The phenomenon of spin accumulation can be explained as follows. The driving force for electrical currents is

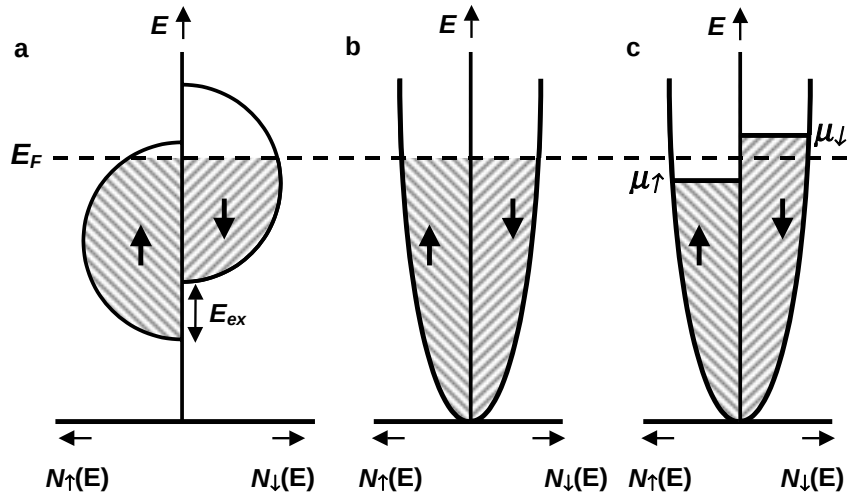

Figure 2.3: *(a) Schematic representation of the spin dependent DOS and occupation of the d states in a ferromagnetic metal. (b) Unpolarized DOS of the free electron like s states in a nonmagnetic metal. (c) Spin accumulation in a nonmagnetic metal: the induced magnetization. The non-equilibrium population of the spin-up and spin-down states is caused by the injection of spin polarized current.*

an electrochemical potential gradient. When this reasoning is reversed one can see that the injection of a spin current in a nonmagnetic metal must be associated with different spin-up and spin-down electrochemical potential gradients. This results in different spin-up ($\mu_\uparrow$) and spin-down ($\mu_\downarrow$) electrochemical potentials, with their difference being largest at the interface. By definition the magnitude of this difference ($\mu_\uparrow - \mu_\downarrow$) is called the spin accumulation or the induced magnetization.

2.4 Spin injection and accumulation in a diffusive conductor

The theory is focussed on the diffusive transport regime, which applies when the mean free path l_e is shorter than the device dimensions. The description of electrical transport in a ferromagnetic metal in terms of a two-current (spin-up and spin-down) model dates back to Mott [2–4]. This idea was followed by Fert and Campbell to describe the transport properties of Ni, Fe and Co based alloys [5–8]. Van Son *et al.* [9] have extended the model to describe transport through transparent ferromagnetic metal-nonmagnetic metal interfaces, as shown in Fig 2.2. A firm theoretical underpinning, based on the Boltzmann transport equation has been given by Valet and Fert [10].

They have applied the model to describe the effects of spin accumulation and spin dependent scattering on the CPP-GMR effect in magnetic multilayers. This standard model allows for a detailed quantitative analysis of the experimental results.

An alternative model, based on thermodynamic considerations, has been put forward and applied by Johnson and Silsbee (JS) [49]. In principle both models describe the same physics, and should therefore be equivalent. However, the JS model has a drawback in that it does not allow a direct calculation of the spin polarization of the current (η in Refs. [49–53]), whereas in the VF model all measurable quantities can be directly related to the parameters of the experimental system [10, 54, 55].

2.4.1 The two channel model

In general, electron transport through a diffusive channel is a result of a difference in the (electro-)chemical potential of two connected electron reservoirs [56]. An electron reservoir is an electron bath in full thermal equilibrium. The chemical potential μ_{ch} is by definition the energy needed to add one electron to the system, usually set to zero at the Fermi energy (this convention is adapted throughout this text), and accounts for the kinetic energy of the electrons. In the linear response regime, i.e. for small deviations from equilibrium ($|eV| < kT$), the chemical potential equals the excess electron particle density n divided by the density of states at the Fermi energy, $\mu_{ch} = n/N(E_F)$. In addition an electron may also have a potential energy, e.g. due to the presence of an electric field $\mathbf{E}$. The additional potential energy for a reservoir at potential V should be added to μ_{ch} in order to obtain the electrochemical potential (in the absence of a magnetic field):

$$\mu = \mu_{ch} - eV \ , \tag{2.7}$$

where e denotes the absolute value of the electron charge.

From Eq. 2.7 it is clear that a gradient of μ, the driving force of electron transport, can result from either a spatial varying electron density ∇n or an electric field $\mathbf{E} = -\nabla V$. Since μ fully characterizes the reservoir one is free to describe transport either in terms of diffusion ($\mathbf{E} = 0$, $\nabla n \neq 0$) or in terms of electron drift ($\mathbf{E} \neq 0$, $\nabla n = 0$). In the drift picture the whole Fermi sea has to be taken into account and consequently one has to maintain a constant electron density everywhere by imposing: $\nabla n = 0$. We use the diffusive picture where only the energy range $\Delta\mu$, the difference in the electrochemical potential between the two reservoirs, is important to describe transport. Both approaches (drift and diffusion) are equivalent in the linear regime and are related to each other via the Einstein relation:

$$\sigma = e^2 N(E_F) D \ , \tag{2.8}$$

where σ is the conductivity and D the diffusion constant. The transport in a ferromagnet is described by spin dependent conductivities:

$$\sigma_\uparrow = N_\uparrow e^2 D_\uparrow, \text{ with } D_\uparrow = \frac{1}{3} v_{F\uparrow} l_{e\uparrow} \tag{2.9}$$

$$\sigma_\downarrow = N_\downarrow e^2 D_\downarrow, \text{ with } D_\downarrow = \frac{1}{3} v_{F\downarrow} l_{e\downarrow} \ , \tag{2.10}$$

where $N_{\uparrow,\downarrow}$ denotes the spin dependent density of states (DOS) at the Fermi energy (E_F), and $D_{\uparrow,\downarrow}$ the spin dependent diffusion constants, expressed in the average spin dependent Fermi velocities $v_{F\uparrow,\downarrow}$, and average electron mean free paths $l_{e\uparrow,\downarrow}$. Throughout this thesis our notation is $\uparrow$ for the majority spin direction and $\downarrow$ for the minority spin direction. Note that the spin dependence of the conductivities is determined by *both* densities of states and diffusion constants. Also in a typical ferromagnetic metal several bands (which generally have different spin dependent densities of states and effective masses) contribute to the transport. However, provided that the elastic scattering time and the inter band scattering times are shorter than the spin flip times (which is usually the case) the transport can still be described in terms of well defined spin up and spin down conductivities.

Because the spin up and spin down conductivities are different, the current in the bulk ferromagnetic metal will be distributed accordingly over the two spin channels:

$$j_\uparrow = \frac{\sigma_\uparrow}{e} \frac{\partial \mu_\uparrow}{\partial x} \tag{2.11}$$

$$j_\downarrow = \frac{\sigma_\downarrow}{e} \frac{\partial \mu_\downarrow}{\partial x} \ , \tag{2.12}$$

where $j_{\uparrow\downarrow}$ are the spin up and spin down current densities. According to Eqs. 2.11 and 2.12 the current flowing in a bulk ferromagnet is spin polarized, with a polarization given by:

$$\alpha_F = \frac{\sigma_\uparrow - \sigma_\downarrow}{\sigma_\uparrow + \sigma_\downarrow}. \tag{2.13}$$

The next step is the introduction of spin flip processes, described by a spin flip time $\tau_{\uparrow\downarrow}$ for the average time to flip an up-spin to a down-spin, and $\tau_{\downarrow\uparrow}$ for the reverse process. Particle conservation requires:

$$\frac{1}{e} \nabla j_\uparrow = -\frac{n_\uparrow}{\tau_{\uparrow\downarrow}} + \frac{n_\downarrow}{\tau_{\downarrow\uparrow}} \ , \tag{2.14}$$

$$\frac{1}{e} \nabla j_\downarrow = +\frac{n_\uparrow}{\tau_{\uparrow\downarrow}} - \frac{n_\downarrow}{\tau_{\downarrow\uparrow}} \ , \tag{2.15}$$

with $n_\uparrow$ and $n_\downarrow$ being the excess particle densities for each spin. Detailed balance imposes that:

$$N_\uparrow/\tau_{\uparrow\downarrow} = N_\downarrow/\tau_{\downarrow\uparrow} \ , \tag{2.16}$$

so that in equilibrium no net spin scattering takes place. As pointed out already, usually these spin flip times are larger than the momentum scattering time $\tau_e = l_e/v_F$. The transport can then be described in terms of the parallel diffusion of the two spin species, where the densities are controlled by spin flip processes. It should be noted however that in particular in ferromagnets (e.g. permalloy [27–29]) the spin flip times may become comparable to the momentum scattering time. In this case an (additional) spin-mixing resistance arises [1, 7, 57], which will not be discussed further in this thesis.

Combining Eqs. 2.11, 2.12, 2.14, 2.15, 2.16 and using the Einstein relation (Eq. 2.8) one can find that the effect of the spin flip processes can now be described by the following diffusion equation (assuming diffusion in one dimension only):

$$D\frac{\partial^2(\mu_\uparrow - \mu_\downarrow)}{\partial x^2} = \frac{(\mu_\uparrow - \mu_\downarrow)}{\tau_{sf}}, \tag{2.17}$$

where $D = D_\uparrow D_\downarrow(N_\uparrow + N_\downarrow)/(N_\uparrow D_\uparrow + N_\downarrow D_\downarrow)$ is the spin averaged diffusion constant, and the spin relaxation time τ_{sf} is given by: $1/\tau_{sf} = 1/\tau_{\uparrow\downarrow} + 1/\tau_{\downarrow\uparrow}$. Note that τ_{sf} represents the timescale over which the non-equilibrium spin accumulation $(\mu_\uparrow - \mu_\downarrow)$ decays and therefore is equal to the spin lattice relaxation time T_1 used in the Bloch equations: $\tau_{sf} = T_1 = T_2$, see also §2.8.3 for more details. Using the requirement of (charge) current conservation, the general solution of Eq. 2.17 for a uniform ferromagnetic or nonmagnetic wire is now given by:

$$\mu_\uparrow = A + Bx + \frac{C}{\sigma_\uparrow}exp(-x/\lambda_{sf}) + \frac{D}{\sigma_\uparrow}exp(x/\lambda_{sf}) \tag{2.18}$$

$$\mu_\downarrow = A + Bx - \frac{C}{\sigma_\downarrow}exp(-x/\lambda_{sf}) - \frac{D}{\sigma_\downarrow}exp(x/\lambda_{sf}) \ , \tag{2.19}$$

where we have introduced the spin relaxation length:

$$\lambda_{sf} = \sqrt{D\tau_{sf}}. \tag{2.20}$$

The coefficients A,B,C, and D are determined by the boundary conditions imposed at the junctions where the wires are coupled to other wires. In the absence of interface resistances and spin flip scattering at the interfaces, the boundary conditions are: 1) continuity of $\mu_\uparrow$, $\mu_\downarrow$ at the interface, and

2) conservation of spin-up and spin-down currents $j_\uparrow$, $j_\downarrow$ across the interface.

In the Valet-Fert theory [1, 10] the spin relaxation length (λ_{sf}^{VF}) is defined differently as expressed in Eq. 2.20, namely as: $(\lambda_{sf}^{VF})^2=(1/D_\uparrow + 1/D_\downarrow)^{-1}\tau_{sf}^{VF}$. Here τ_{sf}^{VF} is the spin relaxation time as used in V-F theory. Eq. 2.20 would yield: $\lambda_{sf}^2=([N_\downarrow/D_\uparrow(N_\uparrow + N_\downarrow) + N_\uparrow/D_\downarrow(N_\uparrow + N_\downarrow)]^{-1}\tau_{sf}$. In Ref. [10] the definition of λ_{sf}^{VF} is justified with a reference to Ref. [9], which however does not clarify it. In nonmagnetic metals, where $D_\uparrow = D_\downarrow = D_N$ and $N_\uparrow = N_\downarrow$, Eq. 2.20 yields for the diffusion constant of the nonmagnetic metal: $D = D_N$. However the V-F definition in this case yields a different diffusion constant: $D^{VF} = \frac{1}{2}D_N$. Therefore the spin relaxation time $(\tau_{sf})^{VF}$ in the V-F theory corresponds to twice the value of τ_{sf} as defined in Eq. 2.20 in nonmagnetic metals: $(\tau_{sf})^{VF} = 2\tau_{sf} = 2T_1$.

2.5 Spin injection with transparent interfaces

In this section the two current model is applied to a single F/N interface [9] and multi-terminal F/N/F spin valve structures, following the lines of the standard Valet Fert model for CPP-GMR. A resistor model of the F/N/F spin valve structures is presented in order to elucidate the principles behind the reduction of the polarization of the spin current at a transparent F/N interface, also referred to as "conductivity mismatch" [58].

2.5.1 The transparent F/N interface

Van Son *et al.* [9] applied Eqs. 2.18 and 2.19 to describe the spin accumulation and at a transparent F/N interface. By taking the continuity of the spin-up and spin-down electrochemical potentials and the conservation of spin-up and spin down-currents at the F/N interface two phenomena occur. This can be seen in Fig. 2.4 which shows how the spin polarized current (I) in the (bulk) ferromagnetic metal is converted into a non-polarized current in the nonmagnetic metal away from the interface. First a "spin-coupled" interface resistance arises given by:

$$R_{\mathrm{I}} = \frac{\Delta\mu}{eI} = \frac{\alpha_{\mathrm{F}}^2(\sigma_{\mathrm{N}}^{-1}\lambda_{\mathrm{N}})(\sigma_{\mathrm{F}}^{-1}\lambda_{\mathrm{F}})}{(\sigma_{\mathrm{F}}^{-1}\lambda_{\mathrm{F}}) + (1-\alpha_F^2)(\sigma_{\mathrm{N}}^{-1}\lambda_{\mathrm{N}}),} \tag{2.21}$$

where σ_N, σ_F and λ_N, λ_F are the conductivity and spin relaxation length of the nonmagnetic metal region and the ferromagnetic metal region respectively. Note that in a spin valve measurement one would measure a spin dependent resistance $\Delta R = 2R_{\mathrm{I}}$ between parallel and anti-parallel magnetization configuration of the spin valve.

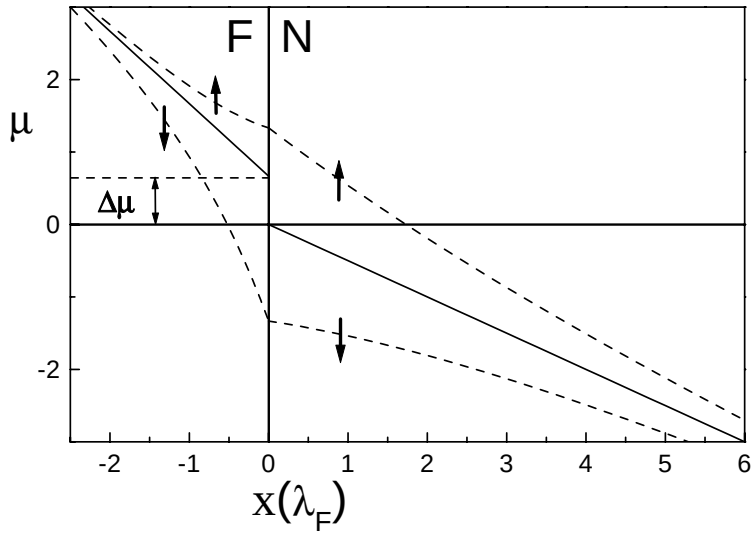

Figure 2.4: *Electrochemical potentials (or densities) of spin-up and spin-down electrons with a current I flowing through an F/N interface. Both spin accumulation as well as spin coupled resistance can be observed (see text). The figure corresponds to* $\lambda_N = 5\lambda_F$.

The second phenomenon is that at the F/N interface the electrochemical potentials $\mu_\uparrow, \mu_\downarrow$ of the spin-up and spin-down electrons are split. This implies that spin accumulation occurs, which has the maximum value at the interface:

$$\mu_\downarrow - \mu_\uparrow = \frac{2\Delta\mu}{\alpha_F} \tag{2.22}$$

with $\Delta\mu$ given by Eq. 2.21.

In addition the expression for the spin polarization of the current at the interface is given by:

$$P = \frac{I_\uparrow - I_\downarrow}{I_\uparrow + I_\downarrow} = \frac{\alpha_F \sigma_N \lambda_F}{\sigma_N \lambda_F + (1-\alpha_F^2)\sigma_F \lambda_N} \tag{2.23}$$

Thus the above equations show that the magnitude of the spin-coupled resistance, spin accumulation and polarization of the current is essentially limited by ratio of $\sigma_N^{-1}\lambda_N$ and $\sigma_F^{-1}\lambda_F$. Since the condition $\lambda_F \ll \lambda_N$ holds in almost all cases for metallic systems, this implies that the spin relaxation length in the ferromagnetic metal is the limiting factor to obtain a large polarization P. This problem becomes progressively worse, when (high conductivity) metallic ferromagnets are used to inject spin polarized electrons into (low conductivity) semiconductors and has become known as "conductivity mismatch" [58, 59]. Another way to look at it is that the ferromagnetic metal behaves as a very effective spin reservoir because once the

electron has diffused (back) into the ferromagnetic metal its spin is flipped very fast. The proximity of the ferromagnetic metal disturbs therefore a non-equilibrium spin population present inside the nonmagnetic metal.

2.5.2 Multi-terminal F/N/F spin valve structures

In this section the model of spin injection is applied to a non local geometry, which reflects the measurement and device geometry, see Fig. 2.5a and Fig. 3.7b.

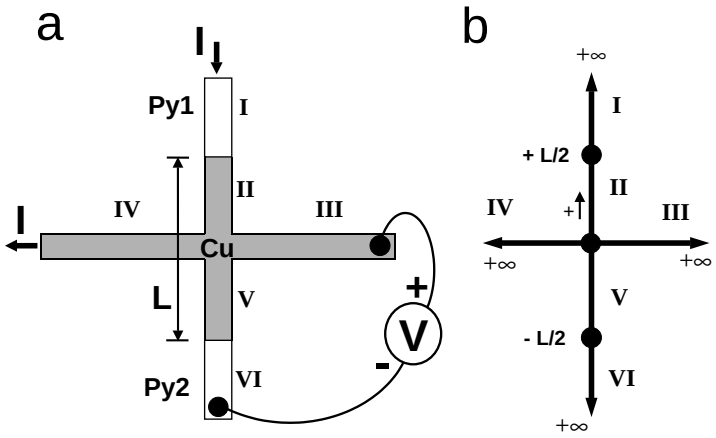

Figure 2.5: *(a) Schematic representation of the multi-terminal spin valve device. Regions* I *and* VI *denote the injecting (F_1) and detecting (F_2) ferromagnetic contacts, whereas regions* II *to* V *denote the four arms of a normal metal cross (N) placed in between the two ferromagnets. A spin polarized current is injected from region* I *into region* II *and extracted at region* IV*. (b) Diagram of the electrochemical potential solutions (Eqs. 2.18 and 2.19) in each of the six regions of the multi-terminal spin valve. The nodes represent the origins of the coordinate axis in the 6 regions, the arrows indicate the (chosen) direction of the positive x-coordinate. Regions* II *and* III *have a finite length of half the ferromagnetic electrode spacing L. The other regions are semi-infinite.*

In the (1-dimensional) geometry of Fig.2.5a 6 different regions can be identified for which Eqs. 2.18 and 2.19 have to be solved according to their boundary conditions at the interface. The geometry is schematically shown in Fig.2.5b, where the 6 different regions are marked with roman letters I to VI. Using Eq. 2.18 for parallel magnetization of the ferromagnetic regions, the equations for the spin-up electrochemical potentials from region I to region VI read (in numerical order):

$$\mu_\uparrow = A - \frac{je}{\sigma_F}x + \frac{2C}{\sigma_F(1+\alpha_F)}exp(-x/\lambda_F) \quad (2.24)$$

$$\mu_\uparrow = \frac{-je}{\sigma_N}x + \frac{2E}{\sigma_N}exp(-x/\lambda_N) + \frac{2F}{\sigma_N}exp(x/\lambda_N) \quad (2.25)$$

$$\mu_\uparrow = \frac{2G}{\sigma_N}exp(-x/\lambda_N) \quad (2.26)$$

$$\mu_\uparrow = \frac{je}{\sigma_N}x + \frac{2G}{\sigma_N}exp(-x/\lambda_N) \quad (2.27)$$

$$\mu_\uparrow = \frac{2H}{\sigma_N}exp(-x/\lambda_N) + \frac{2K}{\sigma_N}exp(x/\lambda_N) \quad (2.28)$$

$$\mu_\uparrow = B + \frac{2D}{\sigma_F(1+\alpha_F)}exp(-x/\lambda_F)\ , \quad (2.29)$$

where $\sigma_\uparrow = \sigma_F(1+\alpha_F)/2$ and A to K are 9 unknown constants. The equations for the spin-down electrochemical potential in the six regions of Fig. 2.5 can be found by putting a minus sign in front of the constants C, D, E, F, H, K, G and α_F in Eqs. 2.24 to 2.29. Constant B is the most valuable to extract from this set of equations, for it gives directly the difference between the electrochemical potential measured with a normal metal probe at the center of the nonmagnetic metal cross in Fig. 2.5a and the electrochemical potential measured with a ferromagnetic voltage probe at the F/N interface of region V and VI. For $\lambda_{sf} >> L$ i.e. no spin relaxation in the nonmagnetic metal of regions II and V, the ferromagnetic voltage probe effectively probes the electrochemical potential difference between spin-up and spin-down electrons at center of the nonmagnetic metal cross. Solving the Eqs. 2.24 to 2.29 by taking the continuity of the spin-up and spin-down electrochemical potentials and the conservation of spin-up and spin down-currents at the 3 nodes of Fig. 2.5b, one obtains:

$$B = -je\frac{\alpha_F^2\frac{\lambda_N}{\sigma_N}e^{-L/2\lambda_N}}{2(M+1)[Msinh(L/2\lambda_N) + cosh(L/2\lambda_N)]}\ , \quad (2.30)$$

where $M = (\sigma_F\lambda_N/\sigma_N\lambda_F)(1-\alpha_F^2)$ and L is the length of the nonmagnetic metal strip in between the ferromagnetic electrodes. The magnitude of the spin accumulation at the F/N interface of region V and VI is given by: $\mu_\uparrow - \mu_\downarrow = 2B/\alpha_F$.

In the situation where the ferromagnets have an anti-parallel magnetization alignment, the constant B of Eq. 2.30 gets a minus sign in front. Upon changing from parallel to anti-parallel magnetization configuration (a spin valve measurement) a difference of $2\Delta\mu = 2B$ will be detected in electrochemical potential between the normal metal and ferromagnetic voltage probe. This leads to the definition of the spin-dependent resistance $\Delta R = \frac{2B}{-ejS}$, where S is the cross-sectional area of the nonmagnetic strip:

$$\Delta R = \frac{\alpha_F^2 \frac{\lambda_N}{\sigma_N S} e^{-L/2\lambda_N}}{(M+1)[M sinh(L/2\lambda_N) + cosh(L/2\lambda_N)]} \ . \tag{2.31}$$

Eq. 2.31 shows that for $\lambda_N << L$, the magnitude of the spin signal ΔR will decay exponentially as a function of L. In the opposite limit, $\lambda_F << L << \lambda_N$ the spin signal ΔR has a 1/L dependence. In this limit and under the constraint that $ML/2\lambda_N >> 1$, Eq. 2.31 can be written as:

$$\Delta R = \frac{2\alpha_F^2 \lambda_N^2}{M(M+1)\sigma_N S L} \ . \tag{2.32}$$

In the situation where there are no spin flip events in the normal metal ($\lambda_N = \infty$) Eq. 2.32 can be written as in an even more simple form:

$$\Delta R = \frac{2\alpha_F^2 \lambda_F^2 / \sigma_F^2}{(1-\alpha_F^2)^2 S L / \sigma_N} \ . \tag{2.33}$$

The important point to notice is that Eq. 2.33 clearly shows that even in the situation when there are no spin flip processes in the normal metal, the spin signal ΔR is reduced with increasing L. The reason is that the *spin dependent* resistance ($\lambda_F/\sigma_F S$) of the injecting and detecting ferromagnets remains constant for the two spin channels, whereas the *spin independent* resistance ($L/\sigma_N S$) of the nonmagnetic metal in between the two ferromagnets increases linearly with L. In both nonmagnetic metal regions II and V (Fig. 2.5) the spin currents have to traverse a total resistance path over a length $\lambda_F + L/2$ and therefore the polarization of the current flowing through these regions will decrease linearly with L and hence the spin signal ΔR. Note that in the regions V and VI no net current is flowing as the opposite flowing spin-up and spin-down currents are equal in magnitude.

Using Eqs. 2.11, 2.12 and 2.24 the current polarization *at the interface* of the current injecting interface can be calculated. The interface current polarization is defined as $P = \frac{j_\uparrow^{int} - j_\downarrow^{int}}{j_\uparrow^{int} + j_\downarrow^{int}}$ and one obtains:

$$P = \alpha_F \frac{M e^{L/2\lambda_N} + 2cosh(L/2\lambda_N)}{2(M+1)[M sinh(L/2\lambda_N) + cosh(L/2\lambda_N)]} \ . \tag{2.34}$$

In the limit that $L >> \lambda_N$ we obtain the polarization of the current at a single F/N interface, see Eq. 2.23:

$$P = \frac{\alpha_F}{M+1} \ . \tag{2.35}$$

Again, Eq. 2.35 shows a reduction of the polarization of the current at the F/N interface, when the spin dependent resistance ($\lambda_F/\sigma_F S$) is much smaller than the spin independent resistance ($\lambda_N/\sigma_N S$) of the nonmagnetic metal as already mentioned in §2.5.1.

The spin signal ΔR^{Conv} can also be calculated for a conventional measurement geometry, see Fig. 3.7a, writing down similar equations and boundary conditions as was done for the non local geometry (Eqs. 2.24 to 2.29). One finds:

$$\Delta R^{Conv} = 2\Delta R \,. \tag{2.36}$$

Eq. 2.36 shows that the magnitude of the spin valve signal measured with a conventional geometry is increased by a factor two as compared to the non local spin valve geometry (see also Eq. 45 of Ref. [54]).

2.5.3 Resistor model of F/N/F spin valve structures

More physical insight can be gained by considering an equivalent resistor network of the spin valve device [60, 61]. In the linear transport regime, where the measured voltages are linear functions of the applied currents, the spin transport for the conventional and non local geometry can be represented by a two terminal and four terminal resistor network respectively. This is shown in Fig. 2.6 for both parallel and anti-parallel configuration of the ferromagnetic electrodes. The resistances $R_\downarrow$ and $R_\uparrow$ represent the resistances of the spin up and spin down channels, which consist of the different spin-up and spin-down resistances of the ferromagnetic electrodes $(R^F_\uparrow, R^F_\downarrow)$ and the spin independent resistance R^{SD} of the nonmagnetic wire in between the ferromagnetic electrodes. From resistor model calculations one obtains:

$$R_\uparrow = R^F_\uparrow + R^{SD} = \frac{2\lambda_F}{w(1+\alpha_F)} R^F_\square + \frac{L}{w} R^N_\square \tag{2.37}$$

$$R_\downarrow = R^F_\downarrow + R^{SD} = \frac{2\lambda_F}{w(1-\alpha_F)} R^F_\square + \frac{L}{w} R^N_\square \,, \tag{2.38}$$

where $R^F_\square = 1/\sigma_F h$ and $R^N_\square = 1/\sigma_N h$ are the "square" resistances of the ferromagnet and nonmagnetic metal thin films, w and h are the width and height of the nonmagnetic metal strip. The resistance $R = (\lambda_N - L/2)2R^N_\square/w$ in Fig. 2.6c and Fig. 2.6d represents the resistance for one spin channel in the side arms of the nonmagnetic metal cross over a length $\lambda_N - L/2$, corresponding to the regions IV and V of Fig. 2.5b.

Provided that $\lambda_N \gg L$ the spin dependent resistance ΔR^{Conv} between the parallel (Fig. 2.6a) and anti-parallel (Fig. 2.6b) resistor networks for the conventional geometry can be calculated using Eqs. 2.37 and 2.38. One obtains the familiar expression [1, 24]:

$$\Delta R^{Conv} = \frac{(R_\downarrow - R_\uparrow)^2}{2(R_\uparrow + R_\downarrow)}. \tag{2.39}$$

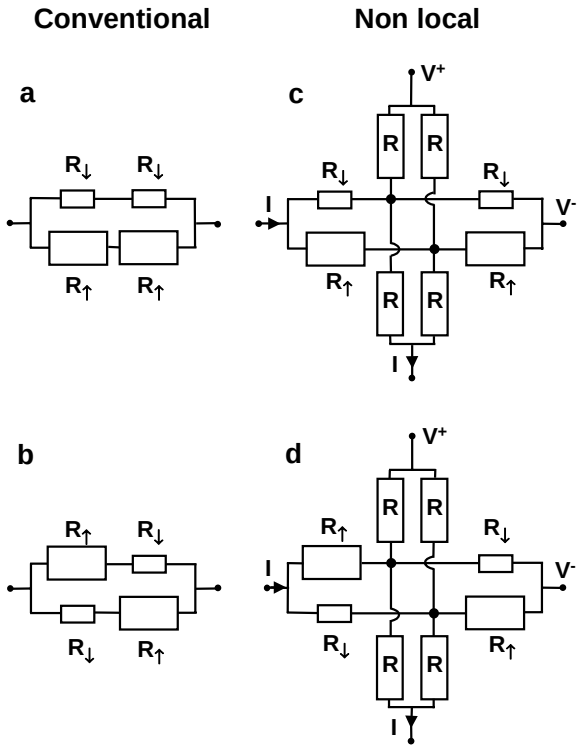

Figure 2.6: *The equivalent resistor networks of the spin valve device. (a) The conventional spin valve geometry in parallel and (b) in anti-parallel configuration. (c) The non-local spin valve geometry in parallel and (d) in anti-parallel configuration.*

For the non local geometry and under the condition $\lambda_N \gg L$ the spin dependent resistance ΔR between the parallel (Fig. 2.6c) and anti-parallel (Fig. 2.6d) resistor network can also be calculated. One obtains:

$$\Delta R = \frac{(R_\downarrow - R_\uparrow)^2}{4(R_\uparrow + R_\downarrow)}. \tag{2.40}$$

Eq. 2.40 again shows that the spin signal measured in a non local geometry is reduced by a factor 2 as compared to a conventional measurement. Provided that $R^F_\uparrow, R^F_\downarrow \ll R^{SD}$ Eqs. 2.37 and 2.38 can be used to rewrite Eq. 2.40 into:

$$\Delta R = \frac{2\alpha_F^2 \lambda_F^2 R_\square^{F\,2}}{(1-\alpha_F^2)^2 L w R_\square^N}\ . \tag{2.41}$$

Using $S = wh$ and replacing the square resistances by the conductivities Eq. 2.41 reduces to Eq. 2.33. A direct relation can now be obtained between the experimentally measured quantities ΔR, $R^N_\square$, $R^F_\square$ and the relevant spin dependent properties of the ferromagnetic metal:

$$R_{\downarrow} - R_{\uparrow} = \sqrt{8\Delta R R_{\square}^{N} \frac{L}{w}} = \frac{4\alpha_F \lambda_F R_{\square}^{F}}{(1-\alpha_F^2)w}. \tag{2.42}$$

Eq. 2.42 shows that the magnitude of the bulk spin dependent resistance of the ferromagnetic electrode can be determined directly from the observable experimental quantities as the length, width and square resistance of the nonmagnetic wire and the spin dependent resistance ΔR.

2.6 Spin injection with tunnel barrier contacts

The presence of tunnel barriers for spin injection is crucial to increase the magnitude of the spin valve signal. They provide high spin dependent resistances as compared to the magnitude of the spin independent resistance in the electrical circuit. The importance manifests itself in two ways.

First, the high spin dependent resistance enhances the spin polarization of the injected current flowing into the Al strip by circumventing the "conductivity mismatch" obstacle [62, 63]. One can therefore consider spin injection via a tunnel barrier as an 'ideal' spin current source, because the spin independent 'load' resistance connected to the terminals of this spin source do not influence the polarization of the source current. This is illustrated in Fig. 2.7a, where a resistor scheme for a F/I/N spin injector is shown.

Second, the high spin dependent resistance causes the electrons, once injected, to have a negligible probability to loose their spin information by escaping into the ferromagnetic metal. One can therefore consider spin detection via a tunnel barrier as an 'ideal' spin voltage probe as the spin relaxation induced by the voltage probe is much weaker than the spin relaxation of the material wherein the non equilibrium spin accumulation or density is probed by the measurement. This is illustrated in Fig. 2.7b, where a resistor scheme for a F/I/N spin detector is shown.

Therefore, in a spin valve experiment where the injection and detection is done via tunnel barriers, the spin direction of the electrons during their time of flight from injector to detector can only be altered by (random) spin flip scattering processes in the N strip itself or in the presence of an external magnetic field, by coherent precession.

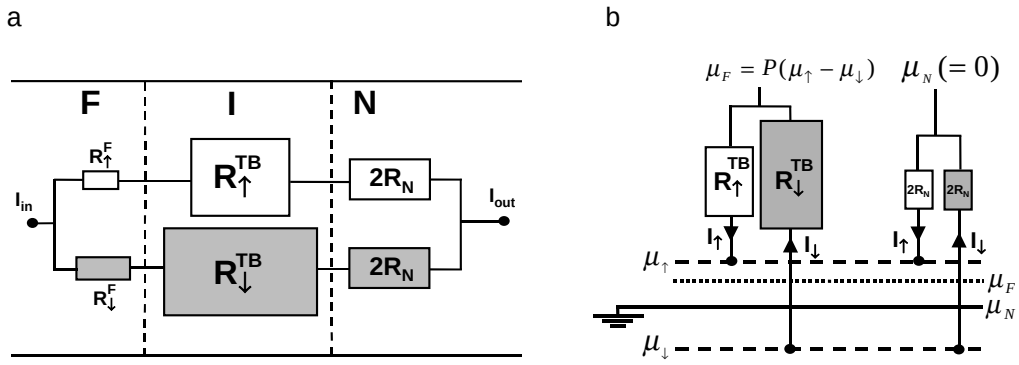

Figure 2.7: *(a) Resistor model of a F/I/N spin injector, showing the resistances experienced by the spin-up and spin-down current over a length $\lambda_F + \lambda_N$ being dominated by the tunnel barrier resistances. (b) Resistor model of a F/I/N spin detector, showing the weak coupling (high resistance) of a F voltage probe to the spin-up and spin-down populations in a nonmagnetic region N of volume V. The 'short' circuiting resistances $2R_N$ represent the spin relaxation due to a nonmagnetic voltage probe strongly (transparent contact) coupled to N.*

2.6.1 The F/I/N injector

The polarization P of the current in the resistor network of the F/I/N spin injector in Fig. 2.7a is given by:.

$$P_{F/I/N} = \frac{(R^F_\downarrow + R^{TB}_\downarrow) - (R^F_\uparrow + R^{TB}_\uparrow)}{(R^F_\uparrow + R^{TB}_\uparrow) + (R^F_\downarrow + R^{TB}_\downarrow) + 4R^N} = \frac{R^{TB}_\downarrow - R^{TB}_\uparrow}{R^{TB}_\downarrow + R^{TB}_\uparrow} \ , \qquad (2.43)$$

where $R^F_\uparrow = \frac{2\lambda_F}{w(1+\alpha_F)} R^F_\Box$, $R^F_\downarrow = \frac{2\lambda_F}{w(1-\alpha_F)} R^F_\Box$, $R^N = \lambda_N/\sigma_N S = \frac{\lambda_N}{w} R^N_\Box$ and $R^{TB}_\uparrow$ ($R^{TB}_\downarrow$) are the spin-up (spin-down) tunnel barrier resistances. The r.h.s. term of Eq. 2.43 is obtained using $(R^{TB}_\uparrow - R^{TB}_\downarrow) \gg (R^F_\uparrow - R^F_\downarrow)$ and $R^{TB}_\uparrow + R^{TB}_\downarrow \gg 4R^N$. Eq. 2.43 shows that the polarization of the current in the nonmagnetic metal is given by the tunnelling polarization P determined by the spin-up and spin-down tunnel barrier resistances.

2.6.2 The F/I/N detector

Here the situation is considered of a ferromagnetic metal strip connected as a voltage probe via a tunnel barrier to a nonmagnetic region N of volume V ($V \ll \lambda_{sf} S$). The F/I/N voltage probe can be represented by resistances $R^{TB}_\uparrow$ and $R^{TB}_\downarrow$, see Fig. 2.7b. By demanding a zero net charge current flow into the voltage probe one can find that the detected potential of the ferromagnetic voltage probe is a weighted average of $\mu_\uparrow$ and $\mu_\downarrow$ in N:

$$\mu_F = \frac{P(\mu_\uparrow - \mu_\downarrow)}{2} + \frac{(\mu_\uparrow + \mu_\downarrow)}{2} \ . \tag{2.44}$$

The term $\frac{(\mu_\uparrow+\mu_\downarrow)}{2}$ in Eq. 2.44 yields the value which would be measured by a nonmagnetic voltage probe ($P = 0$) at the position of the ferromagnetic voltage probe. Usually $\frac{(\mu_\uparrow+\mu_\downarrow)}{2} = 0$ as N is connected to the ground in a real measurement. The F/I/N detector can be considered an 'ideal' spin detector as long as the spin current flowing from ferromagnetic voltage probe via the tunnel barrier into the N region is much smaller the spin relaxation current in N itself (see Eq. 2.53).

Note that a semi-infinite nonmagnetic metal strip connected as a voltage probe to the N region via a transparent contact can be represented by resistances $2R_N = 2\lambda_N/\sigma_N S = \frac{2\lambda_N}{w} R^N_\square$ for both the spin-up and spin-down channel, see Fig. 2.7b. Because both $R^{TB}_\uparrow$ and $R^{TB}_\downarrow$ are much larger than $2R_N$, the opposite flowing spin-up and spin-down currents from ferromagnetic voltage probe via the tunnel barrier to (and from) the N region are much smaller than the spin-up and spin-down currents flowing from (and into) the nonmagnetic voltage probe. The nonmagnetic voltage probe would therefore 'short circuit' the spin-up and spin-down electrochemical potentials existing in N.

2.6.3 The F/I/N/I/F lateral spin valve

Let us consider a 1-D system consisting of an infinite nonmagnetic metal strip (N) and ferromagnetic metal strip (F) at $x = 0$ contacting the nonmagnetic metal strip via a tunnel barrier, see Fig. 2.8. If $x \rightarrow \ \pm\infty$ the spin unbalance in N is completely relaxed. This means that Eqs. 2.18 and 2.19 for $x > 0$ in N reduce to:

$$\mu(x)_\uparrow = \mu_0 \exp(\frac{-x}{\lambda_N}) \quad x > 0 \ , \tag{2.45}$$

$$\mu(x)_\downarrow = -\mu_0 \exp(\frac{-x}{\lambda_N}) \quad x > 0 \ . \tag{2.46}$$

Eqs. 2.45 and 2.46 can be solved by taking the continuity of the spin-up and spin-down electrochemical potentials and the conservation of spin-up and spin down-currents at the injecting contact at $x = 0$:

$$I_\uparrow R^{TB}_\uparrow - I_\downarrow R^{TB}_\downarrow = \frac{2\mu_0}{e} \ , \tag{2.47}$$

$$I_\uparrow = -\frac{I}{2} - \frac{\mu_0 \sigma_N S}{e\lambda_N} \ , \tag{2.48}$$

$$I_\downarrow = -\frac{I}{2} - \frac{\mu_0 \sigma_N S}{e\lambda_N} \ . \tag{2.49}$$

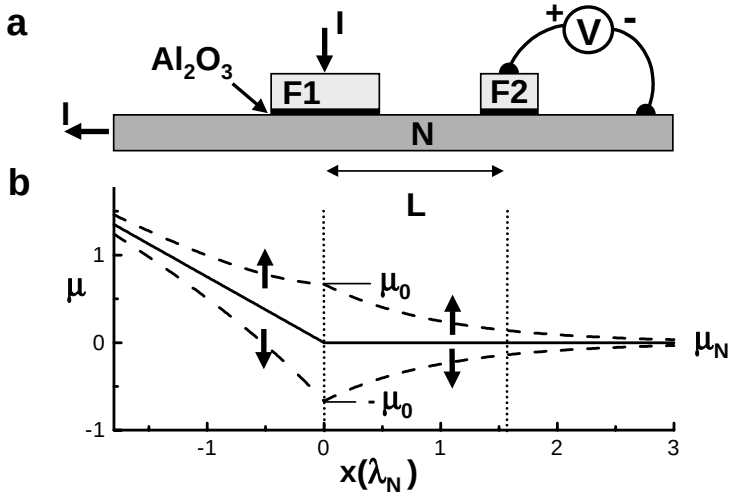

Figure 2.8: *(a) Cross section of a spin valve device, where the ferromagnetic spin injector (F1) is separated from the nonmagnetic metal (N) by an Al_2O_3 tunnel barrier. The second ferromagnetic electrode (F2) is used to detect the spin accumulation at a distance L from the injector. (b) The spatial dependence of the spin-up and spin-down electrochemical potentials (dashed) in the Al strip. The solid lines indicate the electrochemical potential (voltage) of the electrons in the absence of spin injection.*

Note that in deriving Eqs. 2.47, 2.48 and 2.49 the spin-up and spin-down electrochemicals in the ferromagnetic metal have been assumed to be the same. From Eqs. 2.47, 2.48 and 2.49 the magnitude of the spin accumulation $\mu_\uparrow - \mu_\downarrow$ at $x = 0$ yields:

$$\mu_\uparrow - \mu_\downarrow = 2\mu_0 = \frac{IeR_N P}{1 + 2R_N/(R_\uparrow^{TB} + R_\downarrow^{TB})} \ , \tag{2.50}$$

where $R_N = \frac{\lambda_N}{\sigma_N S}$ and $P = \frac{R_\downarrow^{TB} - R_\uparrow^{TB}}{R_\uparrow^{TB} + R_\downarrow^{TB}}$. The denominator of Eq. 2.50 contains the ratio of the spin dependent and spin independent resistances, $2R_N/(R_\uparrow^{TB} + R_\downarrow^{TB})$. If this ratio is large, the spin unbalance is reduced. If the tunnel resistance is sufficiently high ($R_\uparrow^{TB} + R_\downarrow^{TB} \gg R_N$), then:

$$\mu_0 = \frac{IeR_N P}{2} \ . \tag{2.51}$$

At a distance L from the F1 electrode in Fig. 2.8 the induced spin accumulation $(\mu_\uparrow - \mu_\downarrow)$ in the Al strip can be detected by a second F2 electrode via a tunnel barrier. Using Eqs. 2.45, 2.46, 2.51 and 2.44 the magnitude of the output signal (V/I) of the F2 electrode relative to the Al voltage probe at distance L from F1 can be calculated:

$$\frac{V}{I} = \frac{\mu_F - \mu_N}{eI} = \pm \frac{P^2 \lambda_{sf}}{2S\sigma_N} \exp(\frac{-L}{\lambda_{sf}}) \,, \tag{2.52}$$

where $\mu_N = (\mu_\uparrow + \mu_\downarrow)/2$ is the measured potential of the Al voltage probe and the + (-) sign corresponds to a parallel (anti-parallel) magnetization configuration the ferromagnetic electrodes. Eq. 2.52 shows that in the absence of a magnetic field the output signal decays exponentially as a function of L [52, 64].

2.6.4 Injection/relaxation approach

Another way to arrive at Eq. 2.52 is to balance the injection and relaxation rate right underneath the injector ($x = 0$) as used in Refs. [51–53]. In steady state the injection and relaxation rates should be equal:

$$\frac{I_\uparrow - I_\downarrow}{e} = \frac{\Delta n \hat{V}}{\tau_{sf}} \,, \tag{2.53}$$

where $\hat{V} = S \cdot 2\lambda_{sf}$ denotes the volume in which the spin unbalance is present and $\Delta n = n_\uparrow - n_\downarrow = (\mu_\uparrow - \mu_\downarrow)N(E_F)/2 = \mu_0 N(E_F)$ is the difference in electron density of spin up and down electrons. Here use is made of the fact that the total number of excess spin particles is given by $S\int_{-\infty}^{\infty} \Delta n(x)dx = 2S\int_0^\infty \Delta n(0) \exp\left(\frac{-x}{\lambda_{sf}}\right) dx = 2S\lambda_{sf}\Delta n(0)$. Subsequently one finds:

$$\mu_0 = \frac{PI\tau_{sf}}{2eN(E_F)S\lambda_{sf}} = \frac{PIe\lambda_{sf}}{2S\sigma_N} \quad . \tag{2.54}$$

Here the Einstein relation Eq. 2.8 is used to arrive at the last expression. From the general solution of the diffusion equation and the boundary condition $\mu_\uparrow(x)|_{x\to\infty} = 0$ one finds:

$$\mu_\uparrow(x) = \frac{PIe\lambda_{sf}}{2S\sigma_N} e^{\frac{-x}{\lambda_{sf}}} \,. \tag{2.55}$$

The detector potential, see Eq. 2.44, is therefore given by Eq. 2.52.

To arrive at the result obtained by Johnson (Refs. [51, 52, 65]) one has to take a finite volume $V = L \cdot S$. Using Eq. 2.53 one obtains:

$$\mu_0 = \frac{PI\tau_{sf}}{eN(E_F)V} = \frac{PIe\lambda_{sf}^2}{\sigma_N SL} \quad . \tag{2.56}$$

Using Eq. 2.44, the spin valve resistance for a nonmagnetic strip of a finite volume V would than be given by:

$$\Delta R = 2\mu_F/Ie = 2P\mu_0/Ie = 2\frac{P\lambda_{sf}^2}{\sigma_N SL} \quad . \tag{2.57}$$

Eq. 2.57 yields the expression obtained in Refs. [51, 52, 65]. Note that in order to arrive at Eq. 2.57 one has to assume spin detection via tunnel barrier contacts.

2.7 Conduction electron spin relaxation in nonmagnetic metals

The fact that a spin can be flipped implies that there is some mechanism which allows the electron spin to interact with its environment. In the absence of magnetic impurities in the nonmagnetic metal, the dominant mechanism that provides for this interaction is the spin-orbit interaction, as was argued by Elliot and Yafet [66, 67]. When included in the band structure calculation the result of the spin-orbit interaction is that the Bloch eigen functions become linear combinations of spin-up and spin-down states, mixing some spin-down character into the predominantly spin-up states and vice versa [68]. Using a perturbative approach Elliot showed that a relation can be obtained between the elastic scattering time (τ_e), the spin relaxation time (τ_{sf}) and the spin orbit interaction strength defined as $(\lambda/\Delta E)^2$:

$$\frac{\tau_e}{\tau_{sf}} = a \propto (\frac{\lambda}{\Delta E})^2 \, , \tag{2.58}$$

where λ is the atomic spin-orbit coupling constant for a specific energy band and ΔE is the average energy separation from the considered (conduction) band to the nearest band which is coupled via the atomic spin orbit interaction constant. Yafet has shown that Eq. 2.58 is temperature independent [67]. Therefore the temperature dependence of $(\tau_{sf})^{-1}$ scales with the temperature behavior of the resistivity being proportional to (τ_e^{-1}). For many clean metals the temperature dependence of the resistivity is dominated by the electron-phonon scattering and can to a good approximation be described by the Bloch-Grüneisen relation [69]: $(\tau_{sf})^{-1} \sim T^5$ at temperatures below the Debye temperature T_D and $(\tau_{sf})^{-1} \sim T$ above T_D. Using data from CESR experiments, Monod and Beuneu [70, 71] showed that $(\tau_{sf})^{-1}$ follows the Bloch-Grüneisen relation for monovalent alkali and noble metals. In Fig. 2.9 their results are replotted for Cu and Al, using the revised scaling as applied by Fabian and Das Sarma [68]. In addition, data points for Cu and Al at $T/T_D \approx 1$ from the spin injection experiments described in Chapters 5 and 6 are plotted, using the calculated spin orbit strength parameters from Ref. [70]: $(\lambda/\Delta E)^2 = 2.16 \cdot 10^{-2}$ for Cu and $(\lambda/\Delta E)^2 = 3 \cdot 10^{-5}$ for Al.

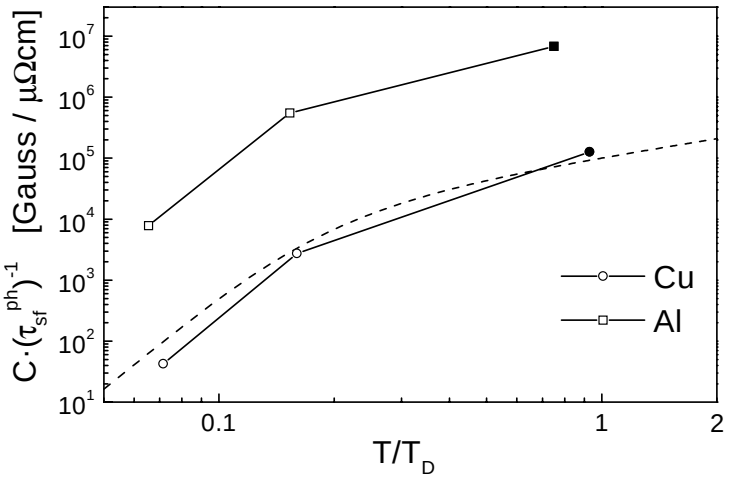

Figure 2.9: *The (revised) Bloch-Grüneisen plot [68]. The quantity* $C \cdot (\tau_{sf}^{ph})^{-1}$ *is plotted versus the reduced temperature* T/T_D *on logarithmic scales. C represents a constant which links* $(\tau_{sf}^{ph})^{-1}$ *to the (original) plotted width of a CESR resonance peak, normalized by the spin orbit strength* $(\lambda/\Delta E)^2$ *and the resistivity* ρ_D *at* $T = T_D$*:* $C = (\gamma(\lambda/\Delta E)^2\rho_D)^{-1}$*. Here* $(\tau_{sf}^{ph})^{-1}$ *is the phonon induced spin relaxation rate,* γ *is the Larmor frequency and* T_D *is the Debye temperature. Values* $\rho_D = 1.5 \cdot 10^{-8}\ \Omega m$ *and* $T_D = 315\ K$ *for Cu and* $\rho_D = 3.3 \cdot 10^{-8}\ \Omega m$ *and* $T_D = 390\ K$ *for Al are used from [69, 72]. The dashed line represents the general Bloch-Grüneisen curve. The open squares represent Al data taken from CESR and the JS spin injection experiment (Refs. [50, 73]). The open circles represent Cu data taken from CESR experiments (Refs. [74–76]). The solid square (Al) and circle (Cu) are values from the spin injection experiments described in this thesis and Refs. [64, 77].*

From Fig. 2.9 it can be seen that for Cu the Bloch-Grüneisen relation is well obeyed, *including* the newly added point deduced from our spin injection experiments at RT ($T/T_D = 0.9$). For Al however the previously obtained data points as well as the newly added point from the injection experiments at RT ($T/T_D = 0.75$) are deviating from the general curve, being about two orders of magnitude larger than the calculated values based on Eq. 2.58 and the Bloch-Grüneisen relation. Note that data points for the Bloch-Grüneisen plot shown in Fig. 2.9 cannot be extracted from the spin injection experiments at $T = 4.2$ K (Chapters 5 and 6), because the impurity (surface) scattering rate is dominating the phonon contribution at $T = 4.2$ K.

Fabian and Das Sarma have resolved the discrepancy for Al in Fig. 2.9 by pointing out that so called 'spin-hot-spots' exist at the Fermi surface of poly valent metals (like Al). Performing an ab initio pseudo potential band structure calculation of Al they showed that the spin flip contribution of

these (small) spin-hot-spot areas on the (large) Fermi surface dominate the total spin flip scattering rate $(\tau_{sf})^{-1}$, making it a factor of 100 faster than expected from the Elliot-Yafet relation [11, 78, 79]. A simplified reasoning for the occurrence of these spin-hot-spots is that in poly valent metals the Fermi surface can cross the first Brillioun zone making the energy separation ΔE in Eq. 2.58 between the (conduction) band to the spin orbit coupled band much smaller at these (local) crossings and hence result in a larger spin orbit strength $(\lambda/\Delta E)^2$. The newly added data point in Fig. 2.9 for Al shows that the under estimation of the spin orbit strength also holds at RT $(T/T_D = 0.75)$. However it is in excellent agreement with the theoretically predicted spin relaxation time at RT ([11]) as will be discussed in Chapter 5.

2.8 Electron spin precession

A (rotating) spinning top will not fall to the ground under the influence of gravity, but rather start to circulating trajectory which is called precession. The gravitational force will exert a torque $\mathbf{T}$ on the spinning top which makes angular momentum vector $\mathbf{L}$ to describe a trajectory which forms the surface of a cone on completing a full cycle. The top angle of the cone is determined by the angle θ between the direction of the gravitational force F_g and $\mathbf{L}$. The precession frequency ω_p of a spinning top (or gyroscope) under the action of a torque $\mathbf{T}$ is:

$$\omega_p = \frac{|\mathbf{T}|}{|\mathbf{L}| \sin\theta} \tag{2.59}$$

A similar phenomenon occurs with the electron spin under the influence of a (perpendicular) magnetic field $\mathbf{B}_\perp$. The $\mathbf{B}_\perp$-field will exert a torque on the spin equal to $\mathbf{T} = -\mu_B B_\perp \sin\theta$ which will make the electron spin precess, a phenomenon known as the Larmor precession. Here $g\mu_B/2$ is the spin magnetic moment associated with the spin angular momentum $\mathbf{S}$, g is the g-factor and μ_B is the Bohr magneton. The precession frequency, known as the Larmor frequency, of the electron spin becomes:

$$\omega_L = -\frac{g\mu_B B_\perp}{\hbar} \ , \tag{2.60}$$

where $\hbar$ is Planck's constant divided by 2π.

2.8.1 The ballistic case

This section applies only to a strictly 1D-ballistic channel as was shown to be a basic requirement for the originally proposed spin FET device by Datta and Das [80, 81]. If a perpendicular field is applied to the initial direction of

the spin, the spin signal will be modulated by the precession. The injected electron spins from F1 into the N strip are exposed to a magnetic field $B\perp$, directed perpendicular to the substrate plane and the initial direction of the injected spins being parallel to the long axes of F electrodes. Because $B\perp$ alters the spin direction of the injected spins by an angle $\phi = \omega_L t$ and the F2 electrode detects their projection onto its own magnetization direction (0 or π), the spin accumulation signal will be modulated by $cos(\phi)$. Here t is the time of flight of the electron travelling from F1 to F2, which for a single mode ballistic channel would be single valued. Assuming there is no backscattering at the interfaces, the observed modulation of the output signal as a function of $B\perp$ would be a perfect cosine function, as is shown in Fig. 2.10.

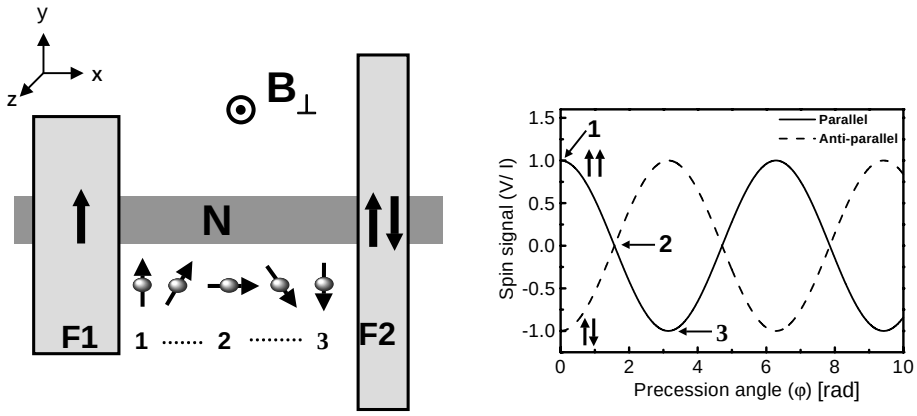

Figure 2.10: *Oscillatory modulation of the spin valve signal (V/I) in a ballistic nonmagnetic metal or semiconductor strip N. The label 1,2 and 3 refer to a precession angle of 0, 90 and 180 degrees.*

For a parallel ↑↑ (anti-parallel ↑↓) configuration we observe an initial positive (negative) signal, which drops in amplitude as $B\perp$ is increased from zero field. The parallel and anti-parallel curves cross each other where the angle of precession is 90 degrees and the output signal is zero. As $B\perp$ is increased beyond this field, we observe that the output signal changes sign and reaches a minimum (maximum) when the angle of precession is 180 degrees, thereby effectively converting the injected spin-up electrons into spin-down electrons and *vice versa*. Note that in this description the spin is considered as a classical object, i.e. the quantum mechanical phase of the spin is ignored.

2.8.2 The diffusive case

Since our metal is diffusive, the travel or diffusion time t between injector and detector is not unique. Diffusive transport implies that there are many

different paths which can be taken by the electrons in going from F1 to F2. Therefore a spread in the diffusion times t occurs and hence a spread in precession angles $\phi = \omega_L t$.

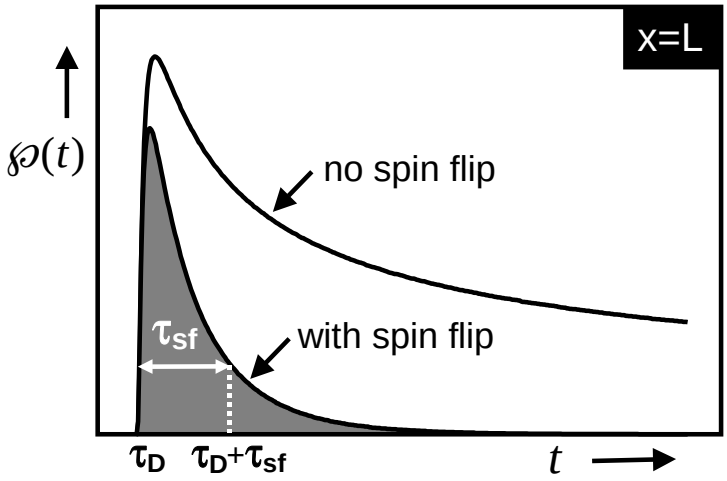

Figure 2.11: *Probability per unit volume that, once an electron is injected, will be present at $x = L$ without spin flip ($\wp(t)$) and with spin flip ($\wp(t) \cdot exp(-t/\tau_{sf})$), as a function of the diffusion time t.*

In an (infinite) diffusive 1D conductor the diffusion time t from F1 to F2 has a broad distribution $\wp(t)$:

$$\wp(t) = \sqrt{1/4\pi Dt} \cdot exp(-L^2/4Dt) \ , \tag{2.61}$$

where $\wp(t)$ is proportional to the number of electrons per unit volume that, once injected at the F1 electrode (x=0), will be present at the Co2 electrode ($x = L$) after a diffusion time t. In Fig. 2.11 $\wp(t)$ is plotted as a function of t, showing that long diffusion times t ($t \gg \tau_D$) still have a considerable weight. Here $\tau_D = \frac{L^2}{2D}$ corresponds to the peak position in $\wp(t)$ ($\frac{\delta\wp(t)}{\delta t} = 0$). So even when τ_{sf} is infinite the broadening of diffusion times will destroy the spin coherence of the electrons present at F2 and hence will lead to a decay of the output signal.

However, spin relaxation by spin flip processes should be taken into account as well. The chance that the electron spin has not flipped after a diffusion time t is equal to $\exp(-t/\tau_{sf})$. If we multiply $\wp(t)$ with this relaxation factor we obtain the probability (per unit volume) that an excess spin particle is located at $x = L$ after a diffusion time t, see Fig. 2.11. Taking into account spin flip results in a much smaller weight for the long diffusion times t ($t \gg \tau_D$) as compared to the original distribution $\wp(t)$ without spin

flip. The damped probability peaks at approximately the same value as $\wp(t)$, i.e. at $\tau_D = \frac{L^2}{2D}$, if τ_D and τ_{sf} are assumed to be in same order of magnitude.

Because of the diffusive broadening all individual electrons can have different precession angles $\phi = \omega_L t$ and therefore the output signal (V/I) is a summation of all contributions of the electron spins over all diffusion times t. This results in a spread of precession angles $\Delta\phi = \omega_L(B_\perp)t$ and hence a damping of the spin signal. However, in the experiment one would like to observe a sign reversal before the spin signal is completely smeared by the diffusive broadening. To see this sign reversal, the spread in precession angles $\Delta\phi$ should be smaller than π, whereas at the same time the average precession angle should be larger than π:

$$\omega_L(B_\perp^{max})\tau_{sf} \leq \pi \ , \tag{2.62}$$

$$\omega_L(B_\perp^{max})\tau_D \geq \pi \ , \tag{2.63}$$

where $B_\perp^{max}$ is the maximum field that is applied. Combining Eqs. 2.62 and 2.63 one immediately finds that these 2 conditions are satisfied when $\tau_D \geq \tau_{sf}$ or:

$$L \geq \sqrt{2}\ \lambda_{sf} \ . \tag{2.64}$$

Note that Eqs. 2.62 - 2.64 are only hand waving results.

Now the output voltage V as a function of the applied field $B_\perp$ can be calculated. The first step is to calculate the number of excess spins with their magnetic moment along the y-direction (see Fig. 2.10) in the normal metal parallel to the detector. This number consists of a summation of all injected spins arriving at F2. Therefore the injection rate PI/e has to be multiplied by probability distribution $\wp(t)\exp(-t/\tau_{sf})$ times the rotation around the z-axis $\cos(\omega_L t)$. This product has to be integrated over all diffusion times t and one obtains:

$$n_\uparrow - n_\downarrow = \frac{IP}{eS}\int_0^\infty \wp(t)\cos(\omega_L t)\exp\left(\frac{-t}{\tau_{sf}}\right)dt \ . \tag{2.65}$$

By using Eq. 2.44 and by noting that $\mu_\uparrow - \mu_\downarrow = \frac{2}{N(E_F)}(n_\uparrow - n_\downarrow)$ the output voltage for a parallel (+) and anti-parallel (-) magnetization configuration of the ferromagnetic electrodes becomes:

$$V(B_\perp) = \pm I\frac{P^2}{e^2 N(E_F)S}\int_0^\infty \wp(t)\cos(\omega_L t)\exp\left(\frac{-t}{\tau_{sf}}\right)dt \ . \tag{2.66}$$

Using the program *Mathematica*^{TM} the integral

$$Int(B\perp) = \int_0^\infty \wp(t)\cos(\omega_L t)\exp\left(\frac{-t}{\tau_{sf}}\right)dt \tag{2.67}$$

can be solved and the obtained expression is:

$$Int(B\perp) = Re\,(\frac{1}{2\sqrt{D}}\frac{\exp\left[-L\sqrt{\frac{1}{D\tau_{sf}} - i\frac{\omega_L}{D}}\right]}{\sqrt{\frac{1}{\tau_{sf}} - i\omega_L}})\,. \tag{2.68}$$

Eq. 2.68 shows that in the absence of precession ($B_\perp = 0$) the exponential decay of Eq. 2.52 is recovered. It can also be shown by using standard goniometric relations that Eq. 2.68 is identical to the solution describing spin precession obtained by solving the Bloch equations with a diffusion term [82]. This will be discussed in the §2.8.3.

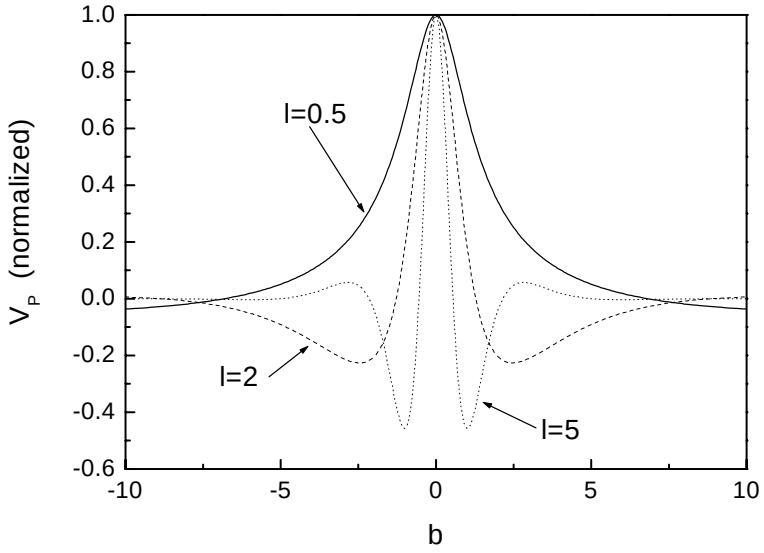

Figure 2.12: *Precession signal. V_P is plotted as a function of the reduced magnetic field parameter b for several values of the reduced injector-detector separation l (see text for their definition)*

The shape of the graph of $V(B_\perp)$ as a function of $B_\perp$ depends on both the spin relaxation length and the diffusion constant of the normal metal. In Fig. 2.12 the precession signal V_P for parallel magnetization is plotted as a function of the reduced field b for several values of the reduced injector-detector separation l, where l, b are defined as:

$$b \equiv \omega_L \tau_{sf}\ , \tag{2.69}$$

$$l \equiv \sqrt{\frac{\tau_D}{\tau_{sf}}} = \frac{\sqrt{2}}{2}\frac{L}{\lambda_{sf}}\ , \tag{2.70}$$

respectively. For $l = 0.5$ the signal is almost critically damped since the condition in Eq. 2.64 is not satisfied.

2.8.3 The magnetic picture

It is convenient to express a spin unbalance in terms of the electrochemical potential since both injection and detection are electrical. However, a spin accumulation is accompanied by a net magnetization $\mathbf{M}_n$. If there is any interaction with internal or external magnetic fields it might be more handy to express a spin accumulation in terms of $\mathbf{M}_n$. Also, since $\mathbf{M}_n$ is a vector, there are no problems in case there is not one practical quantization axis for the whole system, for example if the magnetization axes of injector and detector are not parallel.
Particle density, electrochemical potential, and magnetization are easily related to each other:

$$|\mathbf{M}_n| = \mu_B \Delta n = \mu_B \frac{N(E_F)}{2} \Delta\mu \ . \tag{2.71}$$

Upon injection in the nonmagnetic metal, $\mathbf{M}_n$ is parallel to the magnetization of the injector $\mathbf{M}_n$ whereas during transport the magnetization direction might change as a result of interaction with a magnetic field. A statistic description of this process in terms of precessing single electrons was the starting point in §2.8. By summing over all travel times weighted by their statistical probability and taking spin flip into account $\mathbf{M}_n(L)$ is calculated.
However one could also start with the macroscopic magnetization $\mathbf{M}_n(0)$ and use the Bloch equations with an added diffusion term to calculate $\mathbf{M}_n(L)$. This approach was adapted by Johnson and Silsbee [47] and we will discuss this approach briefly in the next paragraph.

Bloch equations

Another way to obtain Eq. 2.66 is to solve the Bloch equations with an added diffusion term [47]. Applying the magnetic field in the z-direction (the quantization axis), the magnetization of the F1 and F2 strip along the y-direction and the 1-dimensional diffusion along the x-direction (see Fig. 2.10) the Bloch equations read:

$$\frac{dM_y}{dt} = -\omega_L M_x - \frac{M_y}{T_2} + D\frac{\partial^2 M_y}{\partial x^2} \ , \tag{2.72}$$

$$\frac{dM_x}{dt} = \omega_L M_y - \frac{M_x}{T_2} + D\frac{\partial^2 M_x}{\partial x^2} \ . \tag{2.73}$$

$$\frac{dM_z}{dt} = -\frac{M_z}{T_2} + D\frac{\partial^2 M_z}{\partial x^2} \ . \tag{2.74}$$

Note that in a metal, and in zero field, there is no distinction between the longitudinal "spin lattice" relaxation time T_1 and the transverse "dephasing" relaxation time are equal. The reason is that the energy barrier for T_1 spin flip processes is relatively small compared to the total (kinetic) energy the electrons at the Fermi energy. Johnson and Silsbee have found an analytical solution for this set of equations. They obtain for the detected potential by (a weakly coupled) ferromagnetic voltage probe relative to the ground (nonmagnetic voltage probe) [47]:

$$V_d = \frac{1}{2}P^2\frac{I}{e^2N(E_F)S}\sqrt{\frac{T_2}{2D}}F_1\{b,l\} \ , \tag{2.75}$$

where

$$\begin{aligned} F_1\{b,l\} &= \frac{1}{f(b)}[\sqrt{1+f(b)}cos(\frac{lb}{\sqrt{1+f(b)}}) - \\ &\quad -\frac{b}{\sqrt{1+f(b)}}sin(\frac{lb}{\sqrt{1+f(b)}})]e^{-l\sqrt{1+f(b)}} \ . \end{aligned} \tag{2.76}$$

Here $f(b) = \sqrt{1+b^2}$, $b \equiv \omega_L T_2$ is defined as the reduced magnetic field parameter and $l \equiv \sqrt{\frac{L^2}{2DT_2}}$ is defined as the reduced injector-detector separation parameter. It can be shown by using standard goniometric relations that Eq. 2.66 is identical to the solutions 2.75 and 2.76. In particular, using goniometric relations and some algebra one can find that find:

$$Int(B\perp) = \frac{1}{2}\frac{\sqrt{\tau_{sf}}}{2D}F_1\{b,l\} \ , \tag{2.77}$$

indeed showing that Eq. 2.66 is equal to Eq. 2.75. Furthermore, it shows that indeed $T_2 = T_1 = \tau_{sf}$. The definition of τ_{sf} in this thesis is therefore equal (as it should) to the spin lattice relaxation time T_1 used in the Bloch equations [47, 82].

2.8.4 Modulation of the precession signal in high magnetic fields

In the previous paragraphs of this chapter it was assumed that the magnetization of both injector and detector were and stayed parallel to the y-axis. In practice it turns out that the magnetization of both injector and detector strips are tilted out of the substrate plane with an angle θ by a strong perpendicular field $B_\perp$ in the z-direction, see Fig. 2.10. Here the case is discussed where $\mathbf{M}_{i,d}$ is lifted with an angle θ from the substrate (x-y) plain:

$$\mathbf{e}_i = (0 \quad \cos\theta_1 \quad \sin\theta_1)^T , \tag{2.78}$$

$$\mathbf{e}_d = (0 \quad \cos\theta_2 \quad \sin\theta_2) . \tag{2.79}$$

Here θ_1 is the angle between the magnetization direction of the injector electrode and the substrate (x-y) plane and θ_2 is the angle between the detector electrode and the substrate (x-y) plane. The magnitude of the injected magnetization at the injector electrode at x=0 is $|\mathbf{M}_0| = \mu_B(n_\uparrow - n_\downarrow)$ and using Eq. 2.65 the magnetization at $x = L$ is then given by:

$$\mathbf{M}_L = \frac{\mu_B I P}{eS} \int_0^\infty \wp(t) \exp\left(\frac{-t}{\tau_{sf}}\right) R_z(\omega_L t)\ \mathbf{e}_i\ dt , \tag{2.80}$$

where $\wp(t)$ is equal to Eq. 2.61 and $R_z(\omega_L t)$ denotes the standard matrix for a rotation around the z-axis with the precession angle $\omega_L t$. The electrochemical potential and, hence, the output voltage V, can then be calculated by taking the inner vector product of Eq. 2.80 with $\mathbf{e}_d$. Using Eqs. 2.44 and 2.71 to determine the correct pre-factor one obtains:

$$V(B_\perp, \theta_1, \theta_2) = V(B_\perp)\cos\theta_1 \cos\theta_2 + |V(B_\perp = 0)| \sin\theta_1 \sin\theta_2 , \tag{2.81}$$

where $V(B_\perp)$ is given by Eq. 2.66. The extra cosine terms result in a reduction of the precession signal, whereas the sine terms result in a constant signal (independent of the Lamor frequency). If $\theta_1 = \theta_2 = 90°$, then the magnetization of both the injector and the detector are aligned with the perpendicular field $B_\perp$ and no precession takes place anymore.

2.9 Remarks

The theory above has shown that the description of spin diffusion and precession with the Bloch equations, as applied by Johnson and Silsbee in Refs. [47, 50], is fully consistent with the electron transport approach as described in the previous paragraphs in the limit that the ferromagnetic electrodes are weakly coupled to the nonmagnetic region, i.e. via tunnel barriers. In the opposite regime of transparent contacts one can conclude that the physics of spin injection and the CPP magnetoresistance are essentially the same.

In the general case of arbitrary nature of the electrical contacts and non collinear magnetization of the ferromagnetic electrodes the description of spin and electron transport becomes more complicated due the appearance of a mixing conductance [83, 84].

References

[1] M. A. M. Gijs and G. E. W. Bauer, Advances in Physics **46**, 285 (1997).

[2] N. F. Mott, Proc. Roy. Soc. **153**, 699 (1936).

[3] N. F. Mott, Proc. Roy. Soc. **156**, 368 (1936).

[4] N. F. Mott, Adv. Phys. **13**, 325 (1964).

[5] I. A. Campbell, A. Fert, and A. R. Pomeroy, Phil. Mag. **15**, 977 (1967).

[6] A. Fert and I. A. Campbell, J. de Physique, Colloques **32**, C1 (1971).

[7] A. Fert and I. A. Campbell, J. Phys. F **6**, 849 (1976).

[8] E. P. Wohlfarth, *Ferromagnetic Materials* (North Holland, 1982), chap. 9, review article 'Transport properties of ferromagnets', I. A. Campbell, A. Fert, p. 747.

[9] P. C. van Son, H. van Kempen, and P. Wyder, Phys. Rev. Lett. **58**, 2271 (1987).

[10] T. Valet and A. Fert, Phys. Rev. B **48**, 7099 (1993).

[11] J. Fabian and S. D. Sarma, Phys. Rev. Lett. **83**, 1211 (1999).

[12] K. M. Schep, J. B. A. N. van Hoof, P. J. Kelly, G. E. W. Bauer, and J. E. Inglesfield, Phys. rev. B **56**, 10805 (1997).

[13] K. M. Schep, Ph.D. thesis, Delft University of Technology (1997).

[14] K. Xia, P. J. Kelly, G. E. W. Bauer, I. Turek, J. Kudrnovsky, and V. Drchal, Phys. Rev. B **63**, 064407 (2001).

[15] E. Y. Tsymbal and D. Pettifor, Phys. Rev. B **54**, 15314 (1996).

[16] S. Gasiorowicz, *Quantum physics* (John Wiley & Sons, Inc., 1974).

[17] M. Karplus and R. N. Porter, *Atoms and Molecules* (The Benjamin/Cummings Publishing Company, 1970), ISBN 0-8053-5218-X.

[18] R. M. Bozorth, *Ferromagnetism* (IEEE Magnetics Society Liaison to IEEE Press, 1993).

[19] B. Nadgorny, R. J. Soulen, Jr., M. S. Osofsky, I. I. Mazin, G. Laprade, R. J. M. van de Veerdonk, A. A. Smits, S. F. Cheng, E. F. Skelton, et al., Phys. rev. B Rap. Comm. **61**, R3788 (2000).

[20] D. A. Papaconstantopoulos, *Handbook of the band structure of elemental solids* (Plenum, New York, 1986).

[21] C. Vouille, A. Barthélémy, F. E. Mpondo, A. Fert, P. A. Schroeder, S. Y. Hsu, A. Reilly, and R. Loloee, Phys. Rev. B **60**, 6710 (1999).

[22] R. K. Nesbet, J. Phys. **6**, 449 (1994).

[23] W. K. Butler, X. G. Zhang, D. M. C. Nicholson, and J. M. Maclaren, Phys. Rev. B **52**, 13399 (1995).

[24] J. Bass and W. P. Pratt Jr., J. Mag. Magn. Mater. **200**, 274 (1999).

[25] J.-P. A. B. Doudin, A. Blondel, J. Appl. Phys. **79**, 6090 (1996).

[26] L. Piraux, S. Dubois, A. Fert, and L. Beliard, Eur. Phys. J. B **4**, 413 (1998).

[27] S. Dubois, L. Piraux, J. George, K. Ounadjela, J. Duvail, and A. Fert, Phys. Rev. B **60**, 477 (1999).

[28] S. D. Steenwyk, S. Y. Hsu, R. Loloee, J. Bass, and W. P. Pratt Jr., J. Mag. Magn. Mater. **170**, L1 (1997).

[29] P. Holody, W. C. Chiang, R. Loloee, J. Bass, W. P. Pratt, Jr., and P. A. Schroeder, Phys. Rev. B **58**, 12230 (1998).

[30] Q. Yang, P. Holody, S.-F. Lee, L. L. Henry, R. Loloee, P. A. Schroeder, W. P. Pratt, Jr., and J. Bass, Phys. Rev. Lett. **72**, 3274 (1994).

[31] Q. Yang, P. Holody, R. Loloee, L. L. Henry, W. P. Pratt, Jr., P. A. Schroeder, and J. Bass, Phys. Rev. B **51**, 3226 (1995).

[32] L. Piraux, S. Dubois, C. Marchal, J. Beuken, L. Filipozzi, J. F. Despres, K. Ounadjela, and A. Fert, J. Mag. Magn. Mater. **156**, 317 (1996).

[33] C. H. Marrows and B. Hickey, Phys. Rev. B **63**, 220405 (2001).

[34] M. Julliere, Physics Letters **54A**, 225 (1975).

[35] R. Coehoorn, *Lecture notes 'New magnetoelectronic materials and devices'* (unpublished, 1999), 3 parts.

[36] R. Meservey and P. M. Tedrow, Physics Reports **238**, 173 (1994).

[37] P. LeClair, B. Hoex, H. Wieldraaijer, J. T. Kohlhepp, H. J. M. Swagten, and W. J. M. de Jonge, Phys. Rev. B Rap. Comm. **64**, 100406 (2001).

[38] J. M. de Teresa, A. Barthélémy, A. Fert, J. P. Contour, F. Montaigne, and P. Seneor, Science **286**, 507 (1999).

[39] J. G. Simmons, J. Appl. Phys. **34**, 1763 (1963).

[40] P. LeClair, Ph.D. thesis, Eindhoven University of Technology (2002), ISBN 90-386-1989-8.

[41] M. B. Stears, J. Mag. Magn. Mater. **5**, 167 (1977).

[42] I. I. Oleinik, E. Y. Tsymbal, and D. G. Pettifor, Phys. Rev. B **62**, 3952 (2000).

[43] W. Thomson, Proc. R. Soc. **8**, 546 (1857).

[44] J. Smit, Physica **16**, 612 (1951).

[45] T. G. S. M. Rijks, R. Coehoorn, M. M. de Jong, and W. J. M. de Jonge, Phys. Rev. B **51**, 283 (1995).

[46] R. I. Potter, Phys. Rev. B **10**, 4626 (1974).

[47] M. Johnson and R. H. Silsbee, Phys. Rev. B **37**, 5312 (1988).

[48] J.-P. Ansermet, J. Phys.:Condens. Matter **10**, 6027 (1998).

[49] M. Johnson and R. H. Silsbee, Phys. Rev. B **35**, 4959 (1987).

[50] M. Johnson and R. H. Silsbee, Phys. Rev. Lett. **55**, 1790 (1985).

[51] M. Johnson, Science **260**, 320 (1993).

[52] M. Johnson, Phys. Rev. Lett. **70**, 2142 (1993).

[53] M. Johnson, J. Appl. Phys. **75**, 6714 (1994).

[54] A. Fert and S. Lee, Phys. Rev. B **53**, 6554 (1996).

[55] S. Hershfield and L. Z. Zhao, Phys. Rev. B **56**, 3296 (1997).

[56] S. Datta, *Electronic transport in mesoscopic systems* (Cambridge University Press, Cambridge, 1995).

[57] A. Fert, J. L. Duvail, and T. Valet, Phys. Rev. B **52**, 6513 (1995).

[58] G. Schmidt, D. Ferrand, L. W. Molenkamp, A. T. Filip, and B. J. van Wees, Phys. Rev. B **62**, R4790 (2000).

[59] A. T. Filip, B. H. Hoving, F. J. Jedema, B. J. van Wees, B. Dutta, and G. Borghs, Phys. Rev. B **62**, 9996 (2000).

[60] S. F. Lee, W. P. Pratt, Jr., R. Loloee, P. A. Schroeder, and J. Bass, Phys. Rev. B **46**, 548 (1992).

[61] S. F. Lee, W. P. Pratt, Jr., Q. Yang, P. Holody, R. Loloee, P. A. Schroeder, and J. Bass, J. Magn. Magn. Mater. **118**, L1 (1993).

[62] E. I. Rashba, Phys Rev. B Rap. Com. **62**, R16267 (2000).

[63] A. Fert and H. Jaffrès, Phys Rev. B **64**, 184420 (2001).

[64] F. J. Jedema, H. B. Heersche, A. T. Filip, J. J. A. Baselmans, and B. J. van Wees, Nature **416**, 713 (2002).

[65] M. Johnson, Nature **416**, 809 (2002).

[66] R. J. Elliot, Phys. Rev. **96**, 266 (1954).

[67] Y. Yafet, *Solid State Physics* (Academic, New York, 1963).

[68] J. Fabian and S. D. Sarma, J. Vac. Sci. Technol. B **17**, 1708 (1999).

[69] J. Bass, *Metals: Electronic Transport Phenomena*, vol. 15, Part a of *Landolt-Börnstein* (Springer-Verlag, Berlin, 1982).

[70] F. Beuneu and P. Monod, Phys. Rev. B **18**, 2422 (1978).

[71] F. B. P. Monod, Phys. Rev. B **19**, 911 (1979).

[72] C. Kittel, *Introduction to Solid State Physics* (Wiley 7th edition, New York, 1996).

[73] D. Lubzens and S. Schultz, Phys. Rev. Lett. **36**, 1104 (1976).

[74] S. Schultz and C. Latham, Phys. Rev. Lett. **15**, 148 (1965).

[75] F. Beuneu and P. Monod, Phys. Rev. B **13**, 3424 (1976).

[76] P. Monod and A. Janossy, J. Low Temp. Phys. **26**, 311 (1977).

[77] F. J. Jedema, A. T. Filip, and B. J. van Wees, Nature **410**, 345 (2001).

[78] J. Fabian and S. D. Sarma, Phys. Rev. Lett. **81**, 5624 (1998).

[79] J. Fabian and S. D. Sarma, J. Appl. Phys. **85**, 1999 (5075).

[80] S. Datta and B. Das, Appl. Phys. Lett. **56**, 665 (1990).

[81] H. X. Tang, F. G. Monzon, R. Lifshitz, M. C. Cross, and M. L. Roukes, Phys. Rev. B **61**, 4437 (200).

[82] M. Johnson and R. H. Silsbee, Phys. Rev. B **37**, 5326 (1988).

[83] A. Brataas, Y. V. Nazarov, and G. E. W. Bauer, Phys. Rev. Lett **84**, 2481 (2000).

[84] D. Huertas-Hernando, Y. V. Nazarov, A. Brataas, and G. E. W. Bauer, Phys. Rev. B **62**, 5700 (2000).